




Historical droughts in Southeast Australia recorded in a New South Wales stalagmite

The Holocene
2021, Vol. 31(4) 607–617
© The Author(s) 2020
Article reuse guidelines:
sagepub.com/journals-permissions
DOI: 10.1177/0959683620981717
journals.sagepub.com/home/hol


Nick Scroxtan,^{1,2}  Maureen Walczak,^{2,3} Monika Markowska,⁴
Jian-xin Zhao⁵ and Stewart Fallon⁶

Abstract

The Murray Darling Basin contains 40% of Australia's farms and is subject to multi-year droughts that put severe pressure on southeast Australia's freshwater resources. Yet the long-term frequency, timing and potential severity of these droughts is unknown, as there are few high-resolution paleoclimate records from the basin that extend past the instrumental era. In this study, we investigate the potential of stalagmites from Careys Cave, Wee Jasper, in the Murray-Darling Basin to record past droughts. We use a multiproxy approach of stalagmite stable isotopes, trace element data, and climate reanalysis. We show that (a) stalagmite $\delta^{18}\text{O}$ at this site likely records either local or regional precipitation amount and (b) stalagmite $\delta^{18}\text{O}$ shows reasonable coherence with decadal-scale wet and dry changes in regional rainfall over the last 150 years, including the Federation Drought (1895–1902). Therefore, stalagmites from Wee Jasper can be used to draw regional inferences about past rainfall and have potential to extend the record of past droughts in the Murray Darling Basin beyond the limits of historical data. Extracting such a record will enable a better understanding of the causes of multi-year droughts in the region and consequently better planning, mitigation, and resilience in the basin.

Keywords

Australia, drought, Murray-Darling Basin, Speleothem, stable oxygen isotopes, stalagmite, trace elements, U-Th dating

Received 31 July 2020; revised manuscript accepted 6 November 2020

Introduction

Australia has had three major droughts during the historical period: the Federation Drought (1895–1902), the World War II Drought (1937–1945) and the “Big Dry” or Millennium Drought (1997–2010). The nature of Australia's three major historical droughts are disparate, differing in their severity, spatial footprint and different seasonal rainfall anomalies. Whether the underlying climatic drivers of these droughts are also disparate, driven by climatic teleconnections (Verdon-Kidd and Kiem, 2009), or are largely the result of Indian Ocean variability (Ummenhofer et al., 2009) is under debate. Prior to the instrumental era the frequency of these major multi-year to decadal droughts is almost completely unknown, with poor spatial coverage of the region provided by high-resolution paleoclimate proxies (Neukom and Gergis, 2012).

Modern observations, reanalysis, and modeling studies of rainfall variability in southeast Australia (SEA) suggest that a set of ocean-atmosphere interactions in and between the Pacific (El Niño-Southern Oscillation, ENSO), Indian (Indian Ocean Dipole, IOD) and Southern (Southern Annular Mode, SAM) Oceans influence regional precipitation (Cai et al., 2014; McBride and Nicholls, 1983; Murphy and Timbal, 2008; Timbal and Fawcett, 2013; Ummenhofer et al., 2009). In addition, the paleo-record indicates that the interactions between ENSO, IOD and SAM also influenced past SEA rainfall on multi-decadal and centennial scales. A review of Australian paleoclimate records suggests that Indian Ocean variability dominates over Pacific Ocean variability in the southeast (Gouramanis et al., 2013). Other multi-site studies have indicated potential links between SEA hydroclimate during the last millennium and local and regional temperatures, and suggested a possible ENSO influence (Tyler et al., 2015).

An understanding of controls on decadal-scale drought in SEA is hampered by a lack of available high-resolution records. Paleoclimate records that do exist from SEA are frequently restricted by poor resolution and poor age control, especially at the sub-centennial scale over the last 2000 years (Dixon et al., 2017). This prohibits accurate comparisons with the historical record and measured climate indices. Several high resolution SEA climate reconstructions of the last 1000 years do not measure Australian conditions directly but rather infer Australian climate using records from Antarctica (Vance et al., 2013, 2015) and China (McGowan et al., 2009) and assume stationarity in regional teleconnections.

Speleothems may provide these missing records of interannual to decadal scale droughts in SEA. Speleothems, and stalagmites in particular, are long term (growing for thousands of

¹School of Earth Sciences, University College Dublin, Ireland

²Formerly at Research School of Earth Sciences, The Australian National University, Australia

³College of Earth, Ocean and Atmospheric Sciences, Oregon State University, USA

⁴Department of Climate Geochemistry, Max Planck Institute for Chemistry, Germany

⁵Radiogenic Isotope Facility, University of Queensland, Australia

⁶Research School of Earth Sciences, The Australian National University, Australia

Corresponding author:

Nick Scroxtan, School of Earth Sciences, University College Dublin, UCD Science Center West, Belfield, Dublin 4, Ireland.

Email: nick.scroxtan@ucd.ie

Twitter: @stalagnick

years), high resolution (potentially subannual), precisely dateable (frequently $<1\%$ 2σ error) archives that record changing hydroclimate through variable stable isotope ratios and trace element concentrations.

Despite numerous dripwater studies at Yarrangobilly (Coleborn et al., 2016; Markowska et al., 2015; Tadros et al., 2016), Wombeyan (McDonald and Drysdale, 2007; McDonald et al., 2004, 2007) and Wellington (Cuthbert et al., 2014a, 2014b; Jex et al., 2012; Markowska et al., 2016; Rutledge et al., 2014) caves, so far few long-term speleothem results have been produced (Goede et al., 1996; McGowan et al., 2018; Webb et al., 2014). This is in part because speleothems in the area have proven difficult to date precisely (McDonald et al., 2013). In addition, speleothem $\delta^{18}\text{O}$ in parts of SEA may not be controlled by precipitation amount but dominated by in-karst evaporation. For example, in semi-arid zones potential evaporation is higher than local precipitation throughout the year. Stalagmite $\delta^{18}\text{O}$ records from semi-arid caves, for example, Wellington Caves, New South Wales, are likely records of infiltration event frequency, modulated by evaporative enrichment during dry periods, rather than local rainfall amount (Markowska et al., 2020). Further, stalagmites in semi-arid areas are more likely to exhibit discontinuous growth during dry intervals (Markowska et al., 2016) making precise inferences about rainfall variability, and therefore drought frequency, difficult.

More humid ($P > \text{PET}$) areas of SEA, such as the windward slopes of the Great Dividing Range and the Snowy Mountains experience more rainfall and less evaporation than the semi-arid zone and a greater likelihood of effective recharge to karst areas. Thus speleothems from these regions have greater potential for continuous growth and are more likely to be recording antecedent water conditions and karst water balance, and therefore be more sensitive to rainfall amount. Dripwater monitoring studies at Yarrangobilly Caves (75 km south of the study site) indicate that drip-water chemistry is related to Pacific Ocean variability, with both trace elements and stable isotopes correlating well with the Southern Oscillation Index (SOI) (McDonald et al., 2004; Tadros et al., 2016). However, a 2000-year-long speleothem record from Grotto of Oddities at Yarrangobilly Caves was shown to be dominated by changes in moisture source area, and therefore also unsuitable for long-term precipitation amount reconstructions (McGowan et al., 2018).

In this study we investigate a stalagmite from a previously unstudied cave in the temperate zone of SEA: Careys Cave, Wee Jasper, New South Wales. Careys Cave (-35.07°S , 148.66°E) is a show-cave located 50 km northwest of the center of Canberra in the Murrumbidgee catchment of the Murray-Darling river basin (Figure 1a). Rainfall at the nearest weather station of Burrinjuck Dam (BOM ID: 073007), 10 km to the north, is 923 mm per year (Bureau of Meteorology, 2016), substantially higher than the southeast Australian average of 580 mm per year (Timbal and Fawcett, 2013). The additional rainfall is largely due to the orographic effect of the site's location at 393 masl on the western windward slope of the Great Dividing Range (Chubb et al., 2011; Pook et al., 2006). Precipitation at the site occurs all year round, with an increase during the winter months (Figure 2). Potential evapotranspiration at the site is ≈ 650 mm (Matsuura et al., 2009), with higher evapotranspiration in summer months (111 mm/month in January vs 12 mm/month in July). This leads to an annual cycle of moisture deficit and surplus in the soil, with increasing soil moisture during April to June and decreasing soil moisture during November to March.

Methods

The focus of this study is stalagmite CC14-6 (Figure 3). CC14-6 was under an actively dripping stalactite, out of sight of any public walkway and was collected in August 2014. We constructed a concrete replica of CC14-6 using a latex mold to replace the

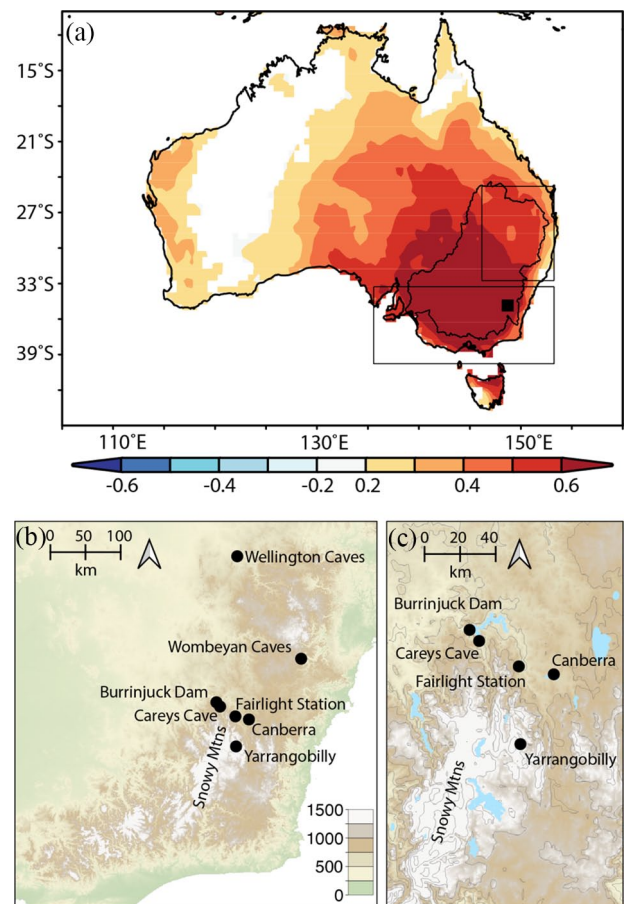


Figure 1. Location maps and local climate relationships. (a) Correlation of hydrological year (July–June) precipitation anomalies at 0.5° resolution with the Wee Jasper gridcell (black square, not to scale). All areas with color have a significance correlation $p < 0.05$. Black boxes denote areas of regional climate correlation in (Timbal and Fawcett, 2013) (southern box) and (Vance et al., 2015) (approximate location, northern box). Correlations calculated using the CRU TS3.23 dataset from 1901 to 2014 (Harris et al., 2014) and the KMNI Climate Explorer (Trouet and Van Oldenborgh, 2013). (b) and (c) Topographic maps indicative of proximity of Careys cave to local weather stations, regional caves, and topographic features. (b) and (c) were generated in QGIS using 9 s digital elevation model with smoothed contours (Hutchinson et al., 2008), and lake shapefiles from 1:2.5 million topographic data (Geoscience Australia, 2003), both from Geoscience Australia on a Creative Commons 4.0 international license.

stalagmite and reduce the visual impact of the stalagmite's removal. A central slab from CC14-6 containing the growth axis was removed and polished. The active stalagmite grew on top of an older speleothem that displayed signs of dissolution and calcite infilling. A shift in drip position in the younger section created two growth axes. The U-Th ages indicate no growth hiatus between the two sections, however to ensure fidelity in the isotope record we avoided flank growth, taking samples only from sections of the stalagmite containing visible horizontal growth layers. This creates a sampling hiatus of approximately 10 mm between the top and bottom section.

Four samples weighing 75–90 mg were milled from CC14-6 for U-Th dating (Figure 3), and analyzed at the University of Queensland using MC-ICP-MS (Hellstrom, 2003; Zhou et al., 2011). Ages were calculated using Isoplot 3.7 (Ludwig, 2012) and the half-lives of (Cheng et al., 2013) and (Jaffey et al., 1971).

Twenty-three additional samples, weighing ~ 5 mg each, were milled from the top-section of CC14-6 for radiocarbon analyses, using the same track milled for stable isotopes (below). Samples were collected at 0.5 mm vertical resolution, with every other

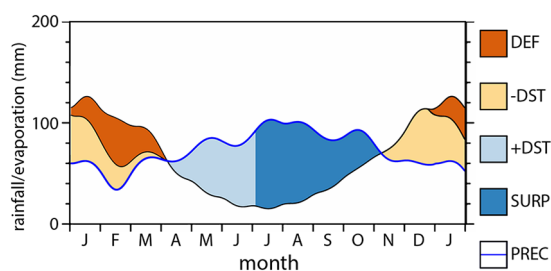


Figure 2. Typical yearly precipitation (blue line) and evaporation (black line) at Wee Jasper. Data from WebWIMP version 1.02 (Matsuura et al., 2009). Assuming default parameters and 150 mm soil moisture store, colored shading indicates state of soil moisture: Orange, DEF, total deficit; Yellow, -DST, draining on soil moisture; Light Blue, +DST, increase in soil moisture; Dark Blue, SURP, surplus of soil moisture.

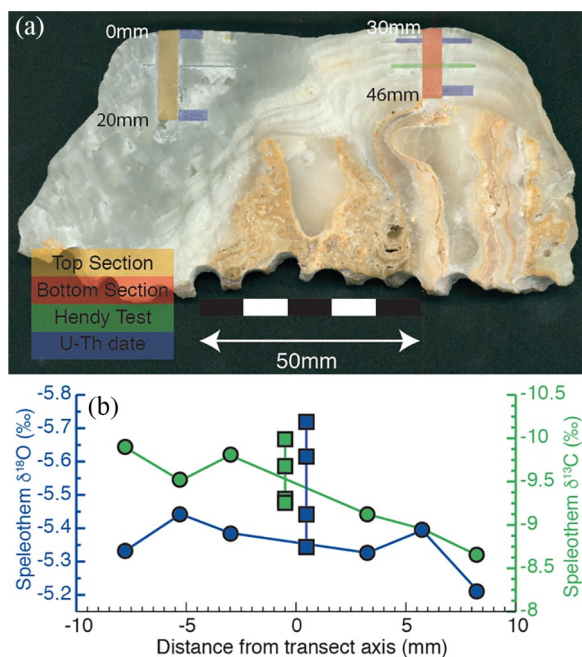


Figure 3. Stalagmite CC14-6. (a) Photograph of the slabbed and polished sampling face with location of milled sections (yellow, red), Hendy Test (green) and U-Th dates (blue) highlighted. (b) Results from the Hendy Test indicating lateral $\delta^{18}\text{O}$ (blue) and $\delta^{13}\text{C}$ (green) measurements (circles) at mid-points of milled sections, alongside stable isotope measurements of coeval milling axis samples (squares).

sample analyzed between 0–8.5 mm and 11.5–20 mm depth, and at full resolution from 8.5 to 11.5 mm depth with the goal of capturing the Southern Hemisphere expression of the 20th century radiocarbon bomb pulse. Radiocarbon analyses were performed at The Australian National University in the Single Stage Accelerator Mass Spectrometry (SSAMS) Lab in the Research School of Earth Sciences following the methods of Fallon et al. (2010).

CC14-6 was milled for carbonate powders at 0.3 mm resolution over 36 mm total growth distance. A total of 179 samples, plus six samples for Hendy tests, were analyzed for $\delta^{18}\text{O}$ and $\delta^{13}\text{C}$ on a Thermo-Finnigan MAT253 gas source isotope ratio mass spectrometer with a coupled Kiel IV carbonate device at The Australian National University. Results are reported according to the VPDB scale using the NBS-19 and NBS-18 standards (Santrock et al., 1985). The long-term lab reported errors are 0.09‰ for $\delta^{18}\text{O}$ and 0.02‰ for $\delta^{13}\text{C}$.

Trace element analysis was conducted on the same powders as the stable isotopes, using Varian Vista AX inductively coupled

plasma atomic emission spectroscopy (ICP-AES) at the Australian National University. Following the methods of Schrag (1999) and de Villiers et al. (2002), 1 mg of carbonate powder was dissolved in 5 ml of 2% HNO_3 and underwent 10 replicate analyses, with bracketing standards, to determine magnesium and strontium concentrations in ratio to calcium (Mg/Ca and Sr/Ca).

Results

Careys Cave is in the Taemas Limestone. The steeply dipping limestone (40° west) leaves about 10–20% of the land surface above the cave as exposed karst with highly variable soil depth. At the time of sample collection ~70–80% of the land cover was grass or introduced gorse, but the surrounding hillsides were open forest, suggesting grass was not the natural cover. Approximately 10% of the land is covered in trees, mainly eucalypts. The speleothem carbon isotope signature of CC14-6 shows a range of -5.8 to -11.0 ‰, within the expected range of speleothem growth under C3 plants.

The rock overburden is approximately 30 m thick. In the far end of the cave, daily visual inspection over 10 years suggests that large formations in the cave become wet a day after significant rainfall or prolonged rainfall over several days (Geoff Kell, 2014, personal communication). These observations need to be quantified by a more thorough monitoring study. Approximately 50 m into the cave, a slight restriction creates a pronounced thermal barrier. A temperature and humidity logger placed beyond the barrier showed no response to diurnal or synoptic scale weather above the internal logger error (0.2°C, 1% relative humidity). Prior to the thermal barrier stalagmite growth is more likely to be influenced by kinetic effects and as such stalagmites appropriate for recent paleoclimate reconstructions should be located beyond the thermal barrier, as is the case for CC14-6. A Hendy Test for kinetic fractionation in CC14-6 indicates no positive correlation between $\delta^{18}\text{O}$ and $\delta^{13}\text{C}$, and no deviation of stable isotope values from coeval axis samples within $+4.5$ – -6.5 mm of the sampled axis (Figure 3b). Since Careys Cave was discovered in the mid 1800s and a wide entrance was installed for public opening in 1968CE, it is possible that stalagmites located closer to the entrance than the thermal barrier and older than 200 years may still be suitable for paleoclimate analysis.

Ages and age model

U-Th dates for CC14-6 are presented in Table 1. Stalagmites from other caves in the region have proven problematic to date due to low uranium concentrations (McDonald et al., 2013). CC14-6 has similarly low uranium concentrations which results in relatively large error. Nevertheless, all ages are in stratigraphic order, and the growth rate is approximately constant in both sections of the stalagmite.

Interpretation of radiocarbon ages (Table 2) as a dating tool in cave environments is complicated due to the incorporation of dead carbon from the dissolved limestone host rock and aged organic matter in the soil, both of which are incorporated into drip waters along with ambient atmospheric CO_2 (Cai, 2005). However, the fraction of modern carbon ($F^{14}\text{C}$) can still provide age constraints using the bomb-pulse method (Genty and Massault, 1997).

The top section of the stalagmite grew over the modern era and shows a dampened bomb-pulse like peak (Figure 4). The first three $F^{14}\text{C}$ measurements are tightly coupled and show a slight decreasing trend ($-0.004 F^{14}\text{C}$), likely related to the Suess (1995) effect. This is followed by a rise in $F^{14}\text{C}$ from ~ 0.687 (19.5–17.25 mm) to peaks of 0.714 (12.15–8.25 mm) before a gradual return to lower values (0.681) toward the top of the stalagmite. Given that both the U-Th ages and dripping stalagmite suggest recent and 20th century growth, we interpret this pattern as reflecting the bomb pulse of radiocarbon associated with nuclear weapons testing in the mid-20th century.

Table 1. U-Th dating results. All ratios refer to activity ratios calculated using decay constants for ^{230}Th and ^{234}U from (Cheng et al., 2013), and the ^{238}U decay constant from (Jaffey et al., 1971). Ages are corrected for detrital ^{230}Th assuming a bulk earth $^{230}\text{Th}/^{232}\text{Th}$ atomic ratio of $4.4 \pm 2.2 \times 10^{-6}$. Samples were dated in April 2015, which was used to calculate ages in CE (Common Era).

Sample ID	Transect distance (mm)	^{238}U (ppm)	$\pm 2\sigma$	^{232}Th (ppb)	$\pm 2\sigma$	$^{234}\text{U}/^{238}\text{U}$ (per mil)	$\pm 2\sigma$	$^{230}\text{Th}/^{238}\text{U}$ (activity)	$\pm 2\sigma$	$^{230}\text{Th}/^{232}\text{Th}$ (activity)	$\pm 2\sigma$	Uncorr. age (ka)	$\pm 2\sigma$	Corr. Age (ka)	Corr. initial $^{234}\text{U}/^{238}\text{U}$ (per mil)	$\pm 2\sigma$	Year (CE)	$\pm 2\sigma$ (years)
CC14-6-U10	1	0.12489	0.00010	0.4504	0.0010	2.4613	0.0033	0.00162	0.00010	1.360	0.083	0.0716	0.0044	0.028	2.4628	0.0033	1987	22
CC14-6-U20	19	0.12606	0.00012	0.7192	0.0013	2.4317	0.0034	0.00311	0.00013	1.654	0.068	0.1395	0.0057	0.070	2.4342	0.0036	1945	35
CC14-6-U33	33	0.08680	0.00013	0.6783	0.0017	2.3034	0.0032	0.00449	0.00045	1.74	0.17	0.213	0.021	0.112	2.3066	0.0035	1903	56
CC14-6-U40	44.5	0.09756	0.00014	0.3356	0.00067	2.3226	0.0056	0.00397	0.00012	3.498	0.107	0.1863	0.0057	0.142	2.3244	0.0057	1873	23

Table 2. Radiocarbon results from CC14-6. $F^{14}\text{C}$ is the fraction modern. Errors are ± 1 sigma.

S-ANU#	Depth (mm)	$F^{14}\text{C}$	\pm
57638	0.25	0.6807	0.0019
57639	1.25	0.6941	0.0017
57704	2.25	0.6725	0.0022
57705	3.25	0.6968	0.0022
57706	4.25	0.6843	0.0023
57707	5.25	0.6960	0.0023
57709	6.25	0.7007	0.0022
57710	7.25	0.6893	0.0047
57711	8.25	0.7187	0.0023
57712	8.75	0.7073	0.0024
57713	9.25	0.6854	0.0022
57714	9.75	0.7082	0.0023
57715	10.25	0.7140	0.0023
57716	10.75	0.7115	0.0027
57717	11.25	0.7065	0.0024
57718	12.25	0.7145	0.0031
57719	13.25	0.7062	0.0024
57720	14.25	0.7031	0.0023
57721	15.25	0.6887	0.0023
57723	16.25	0.6943	0.0024
57724	17.25	0.6856	0.0023
57725	18.25	0.6866	0.0023
57726	19.50	0.6896	0.0022

We modeled the speleothem radiocarbon bomb pulse using the soil model of Markowska et al. (2019). This model consists of four pre-determined carbon reservoirs represented by an array of Weibull distributions to capture carbon in its various availability states, from highly available to very protected. After accounting for the “dead carbon proportion,” a solver function is used to determine the specific and % combination of reservoirs which best fit the measured speleothem $F^{14}\text{C}$, based on the highest r^2 statistic. The input datasets used to model reservoirs were SHZ1_2 (Hua et al., 2013) and SHcal13 (Hogg et al., 2013). Modeled reservoirs range from an instantaneous reservoir (<1 year old) representing carbon from fast organic matter turnover or root respiration, to a physically and chemically protected carbon reservoir which is not bioavailable (<1000 years old). The model produces a best fit using an instantaneous reservoir contributing 7%, a fast reservoir (1–5 years) and an intermediate reservoir (1–40 years) contributing 0% each, and a slow reservoir (1–1000 years) contributing 93%.

The start of the bomb pulse is modeled as half-way between the first $F^{14}\text{C}$ value above the preceding baseline and the preceding data point (Figure 4). The initial sustained rise in $F^{14}\text{C}$ is at 14.25 mm, giving an inflection point at 14.75 mm which the model suggests occurred in year 1959. Stalagmite $F^{14}\text{C}$ variability is controlled by numerous processes, with the modeled best fit response to measured values having an r^2 of 0.36. The radiocarbon model indicates a high dead carbon fraction of 0.29, suggesting the $F^{14}\text{C}$ variability is heavily overprinted by the karst environment in addition to variations in atmospheric $F^{14}\text{C}$. Due to this dampening, peak $F^{14}\text{C}$ is indistinguishable between three datapoints at 12.25, 10.25, and 8.25 mm; we thus use a mean depth of 10.25 mm and a depth uncertainty of 2 mm in our age model. A second-pass radiocarbon model was then run (see Markowska et al., 2019; Figure 5) with the best fit model indicating a date of 1969 for peak $F^{14}\text{C}$.

We constructed an age-model for the top section of CC14-6 using a mixed U-Th and radiocarbon modeling approach (Akers et al., 2019) using the following restrictions:

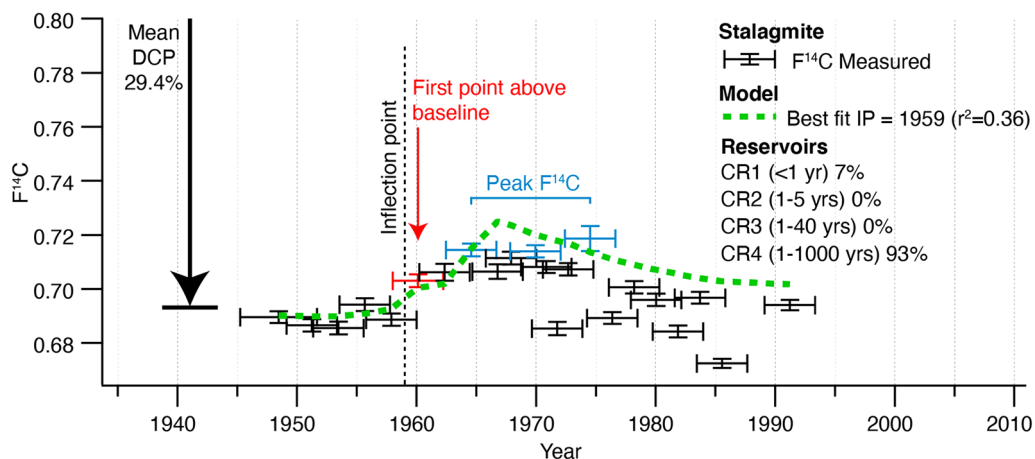


Figure 4. Output of radiocarbon soil model. Error bars indicate stalagmite $F^{14}C$ measurements (Table 2). Model output (green dashed line) shows best fit to results using the first point above baseline (red error bar), inferred inflection point (dashed black line), and the three indistinguishable peak $F^{14}C$ values (blue error bars).

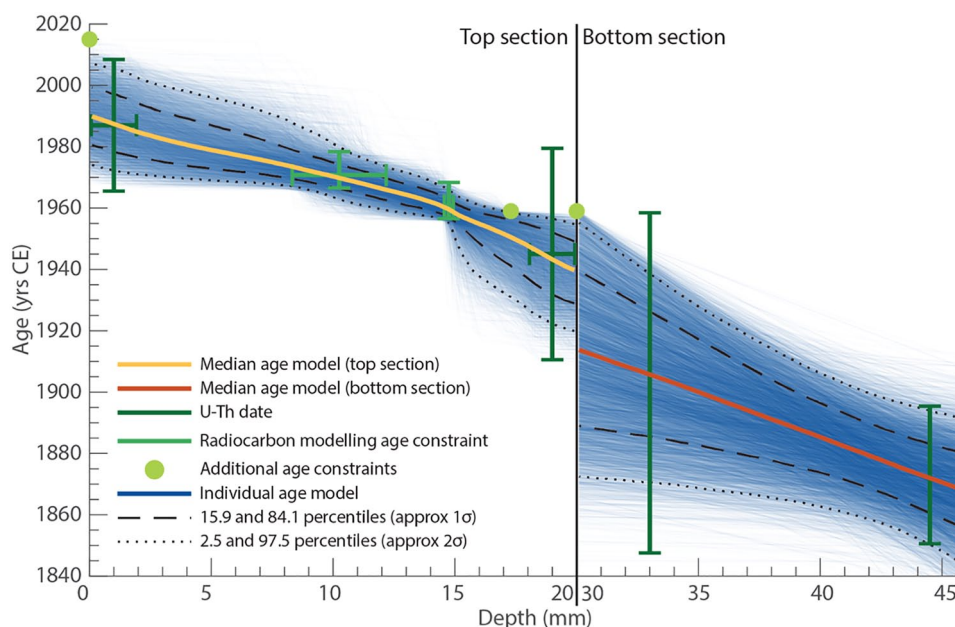


Figure 5. CC14-6 age model. Subset of Monte Carlo simulations (blue lines) through a combination of U-Th (dark green error bars) and radiocarbon (lighter green error bars) ages with Gaussian and Weibull age uncertainty distributions, and uniform depth uncertainty distributions. Additional maximum age constraints in light green (lines and circles). Median age models in yellow (top section of stalagmite) and orange (bottom section of stalagmite). 15.9 and 84.1 percentiles in dashed black lines. 2.5 and 97.5 percentiles in dotted black line.

- (1) Two U-Th dates at 1 and 19 mm depth, of 1987 CE ± 22 years (2σ) and 1945 CE ± 35 years (2σ), with depth errors of ± 1 mm.
- (2) Radiocarbon modeling constraints of 1959 CE at 14.75 mm ± 0.5 mm and 1969 CE at 10.25 mm ± 2 mm based on best fit modeling of the first sustained rise and peak $F^{14}C$ (see below for discussion on uncertainty).
- (3) The oldest three $F^{14}C$ measurements are a decreasing trend and tightly coupled. They occur before the bomb pulse and so no point below 17.25 mm can be younger than 1959.
- (4) The stalagmite was collected in 2014, so the top cannot be younger than 2014.
- (5) The first sustained rise in $F^{14}C$ at 14.75 mm, modeled at 1959, cannot be older than 1955 when the first atmospheric $F^{14}C$ measurements above background in the southern hemisphere were recorded (Hua et al., 2013).
- (6) Peak $F^{14}C$ at 10.25 mm, modeled at 1969, cannot be older than 1965 when atmospheric $F^{14}C$ peaked in the southern hemisphere (Hua et al., 2013).
- (7) Previous studies with sub-annual resolution (Markowska et al., 2019) suggest that it takes 4–41 years for initial and peak radiocarbon to transfer from atmosphere to stalagmite. A long tail of younger ages is therefore possible.

Uncertainty on the modeled radiocarbon-based ages is difficult to quantify as the transfer of ^{14}C atoms from the atmosphere to the stalagmite surface is a process of variable duration controlled by different carbon reservoirs. However, the following additional constraints on the age distribution can be considered:

To accommodate these restrictions the age model for the top section of CC14-6 was created using a modified version of Undatable (Lougheed et al., 2018), a Bayesian age-depth modeling software which allows for uncertainty in depth as well as age. We used an x factor (a between date deposition rate uncertainty coefficient) of 0.3, the highest recommended value, producing the most conservative error bars. Zero bootstrapping ($bootpc=0$) was used as there

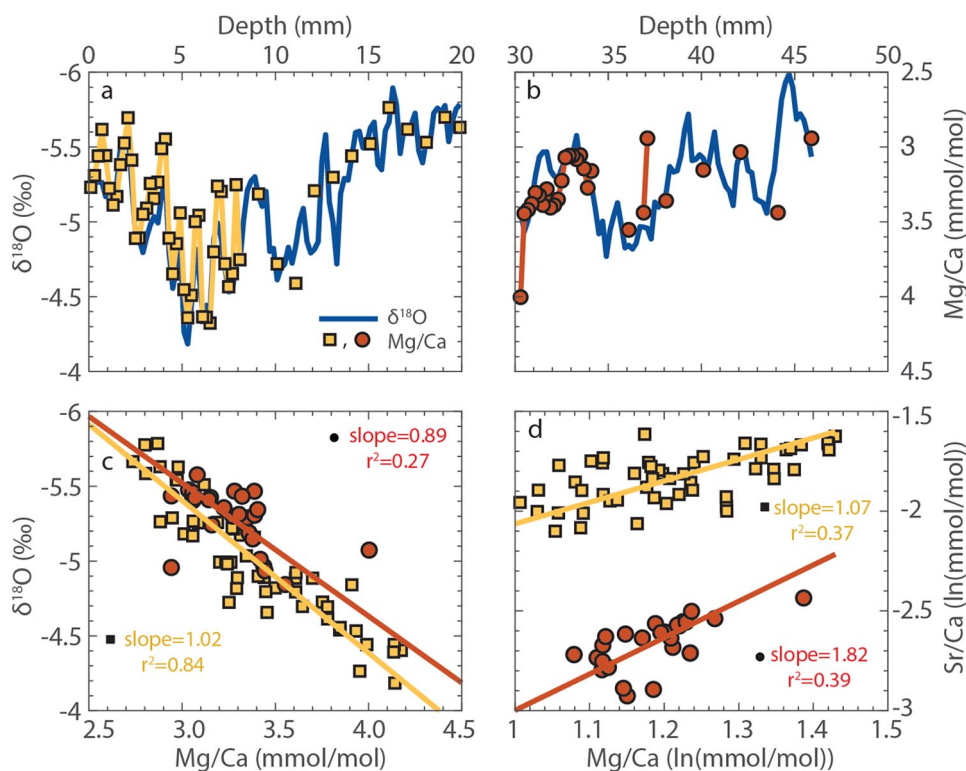


Figure 6. CC14-6 stable isotope and trace element ratios. $\delta^{18}\text{O}$ (blue line) alongside Mg/Ca ratio for (a) Top section and (b) Bottom section. Mg/Ca ratios were determined on the same powders as stable isotope ratios. Continuous measurements connected by lines. (c) Correlation of $\delta^{18}\text{O}$ and Mg/Ca. (d) Correlation of natural logs of Mg/Ca and Sr/Ca ratios used to determine the presence of prior calcite precipitation. In all panels, yellow squares denotes top section of stalagmite, red circles denotes the bottom section.

were only four ages, all in stratigraphic order. Uniform depth uncertainty distributions were used. The modifications to Undatable were as follows: instead of a Gaussian probability density function for the two radiocarbon modeled ages, we used a Weibull probability density function with zero probability at the timing of atmospheric signal (1955, 1965), a peak in probability at the modeled age with best fit (1959, 1969) and a long tail. Because the zero probability minimum age and the maximum likelihood age are already constrained, the median age model is insensitive to the exact Weibull parameters chosen. We used parameters of scale=7 and shape=1.9. A total of 10,000 initial simulations were screened to meet criteria 3 and 4 above. About 7181 age models passed these tests, from which mean and median age models were calculated along with the 2.5, 15.9, and 84.1 and 97.5 percentiles (approx. 1σ and 2σ). As the age models do not produce a Gaussian error distribution at each/any individual depth, we use the median age model as it is likely closer to the peak of the distribution than the mean.

Undatable does not calculate age models with less than three ages. Therefore, we used a simple Monte-Carlo linear interpolation between the two U/Th ages as the age model for the bottom section of the stalagmite. As the bottom section contained no bomb-pulse radiocarbon individual age models were screened for criteria 3 (i.e. no value younger than 1959), until 10,000 successful individual realizations were achieved. Despite the large age uncertainties (1872 ± 23 years at 34.5 mm and 1902 ± 56 years at 23 mm), a linearly interpolated age model (and therefore the most likely age model) has a growth rate of 0.34 mm/yr which is comparable to the average 0.39 mm/yr growth rate of the top section. Again, the median rather than mean age model is used.

Stable isotope and trace element results and interpretation

The CC14-6 $\delta^{18}\text{O}$ and Mg/Ca records are presented in Figure 6. Both records show remarkable coherence. In the older section of

the record, two and a half cycles with minima at 45, 39, and 33 mm are superimposed on an increasing trend. In the younger section of the record, there are relatively stable conditions between 20 and 14 mm, followed by a large amplitude increase and then decrease in values. $\delta^{18}\text{O}$ minima occur at 2 and 16 mm, and a local minima at 8 mm.

Variability in Mg/Ca and Sr/Ca are typically inferred as a proxy for paleohydrology, recording the hydrological response to changing precipitation (Fairchild and Treble, 2009; Fairchild et al., 2000; Johnson et al., 2006). Drier conditions lead to increased low $p\text{CO}_2$ air gaps in the karst, increasing the amount of calcite precipitated upstream of the stalagmite, known as “prior calcite precipitation” (PCP). As calcite preferentially takes up calcium, ratios in the residual fluid and therefore downstream speleothem calcite are enriched in both Mg and Sr, increasing Mg/Ca and Sr/Ca ratios.

If PCP is the major cause of trace element variation, then a predictable gradient between $\ln(\text{Sr}/\text{Ca})$ and $\ln(\text{Mg}/\text{Ca})$ should be observed. The slopes of the younger and older sections of stalagmite are 1.08 ($\sigma=0.13$) and 1.82 ($\sigma=0.31$), respectively (Figure 6d). The younger section ($n=53$) is within the range predicted for PCP by both Sinclair (2011) of 0.88 ± 0.13 and Wassenburg et al. (2020) of 0.709 “or even lower” to 1.45. The older section is outside the Sinclair range and within 2σ of the Wassenburg range. r^2 are similar for both sections: 0.37 and 0.39, respectively. We suggest that PCP is the likely major control on Sr/Ca and Mg/Ca in CC14-6 but recognize that other potential influences may exist (McDonald et al., 2007; Tardos et al., 2016).

The absolute Sr/Ca values are offset between the older and younger growth axes. There are two possible explanations. The first is an absolute change in Sr availability in the new drip pathway. The second is incongruous dissolution of fresh calcite surfaces when switching to a new drip pathway. As incongruous dissolution would also result in an increase in Mg, and an increase $\ln(\text{Mg}/\text{Ca})/\ln(\text{Sr}/\text{Ca})$ gradient, neither of which are observed (Figure 6d) (Sinclair, 2011), we favor the former explanation.

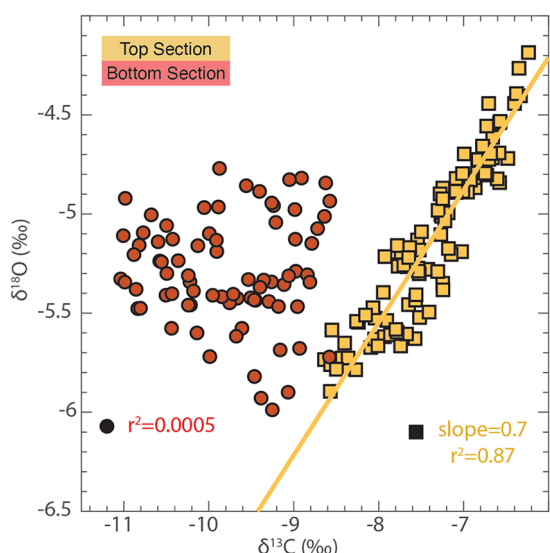


Figure 7. CC14-6 stable isotopes. $\delta^{13}\text{C}$ versus $\delta^{18}\text{O}$ top section (yellow squares) and bottom section (red circles), with geometric mean regression for the top section (yellow line).

The Mg/Ca results show remarkable coherence with the $\delta^{18}\text{O}$ results, both in broad-scale features and finer details of the record (Figure 6). This agreement suggests that CC14-6 $\delta^{18}\text{O}$ record is likely to be recording local effective rainfall amount. Therefore speleothem $\delta^{18}\text{O}$ may be recording local rainfall amount through the amount effect. However, outside of the tropics, the control of speleothem $\delta^{18}\text{O}$ by the “amount effect” cannot be assumed *a priori*, even when $\delta^{18}\text{O}$ is well-correlated to a proxy of local infiltration. Alternative mechanisms include the recharge frequency mechanism, the continental effect, and possible in-cave non-equilibrium effects.

A proposed alternative mechanism for caves elsewhere in New South Wales, the recharge frequency mechanism, suggests cave drip water $\delta^{18}\text{O}$, and therefore speleothem $\delta^{18}\text{O}$, correlates with the time between rainfall events due to evaporation in the karst (Markowska et al., 2016, 2020). In contrast to the Wellington Cave site, Careys Cave is not in the semi-arid zone, and $P > ET$ for most of the year. It is unlikely that the recharge frequency mechanism applies here all year round, but we cannot rule out this mechanism as contributing to stalagmite $\delta^{18}\text{O}$ variability between November and March.

Disequilibrium fractionation may also influence $\delta^{18}\text{O}$ variability. Good correlation between stable isotopes and trace elements (Figure 6) suggests that disequilibrium fractionation is not the dominant control on speleothem $\delta^{18}\text{O}$, or that if it is present, variation in the amount of disequilibrium fractionation is forced by climate, changing $\delta^{18}\text{O}$ in the same direction. The Hendy test (Figure 3) also suggests that disequilibrium fractionation is limited, but the Hendy test is itself limited. Disequilibrium fractionation would also likely cause a correlation between $\delta^{13}\text{C}$ and $\delta^{18}\text{O}$, in the same direction and close to a 2:1 ratio. There is no relationship between $\delta^{18}\text{O}$ and $\delta^{13}\text{C}$ in this bottom section of the stalagmite (Figure 7). The top (younger) section of the stalagmite has a strong correlation between $\delta^{18}\text{O}$ and $\delta^{13}\text{C}$ (Figure 7), which may suggest kinetic processes fractionated the isotopes in the same direction. Together, the Hendy test and change in $\delta^{13}\text{C}/\delta^{18}\text{O}$ indicate that any disequilibrium fractionation is likely to have taken place in the karst, not in the cave environment, and is likely related to the changing karst water balance and processes controlling variable prior calcite precipitation and the Mg/Ca/ $\delta^{18}\text{O}$ relationship.

Alternatively/in addition, speleothem $\delta^{18}\text{O}$ at Careys Cave may record regional rainfall amount through the “continental effect.” Under the continental effect precipitation $\delta^{18}\text{O}$ evolves through a combination of recycling of continental moisture via evaporation

(but not evapotranspiration), and continuing isotopic enrichment through Rayleigh distillation as the air mass cools and precipitates over land (Dansgaard, 1964; Lachniet, 2009). Consequently, rainfall $\delta^{18}\text{O}$ at sites with a long moisture transport path becomes correlated to the cumulative rainfall amount along the moisture transport pathway. Measurements of precipitation $\delta^{18}\text{O}$ in the Snowy Mountains approximately 150 km south of Careys Cave suggest that the continental effect is important in controlling the isotopic composition of rainfall in the region as air masses move across SEA with the prevailing westerly wind (Callow et al., 2014).

Local precipitation amount at Careys Cave is correlated with regional rainfall, determined by correlating local rainfall anomalies with a gridded field using the CRU TS3.23 gridded dataset (Harris et al., 2014) (Figure 1a). The CRU TS3.23 dataset uses high quality weather stations and an existing climatology (1961–1990 baseline) to produce monthly gridded precipitation anomalies at 0.5° resolution, which we averaged to the hydrological year (July–June). Precipitation anomalies at the Careys Cave grid cell were compared to the rest of Australia using the KMNI climate explorer (Trouet and Van Oldenborgh, 2013). Results indicate a correlation ($r > 0.5$, $p < 0.05$) between Careys Cave and the Murray-Darling Basin, especially the southern basin ($r > 0.6$, $p < 0.05$).

In summary: the CC14-6 $\delta^{18}\text{O}/\text{Mg}/\text{Ca}$ relationship suggests an effective recharge control on both proxies. Local precipitation isotopes suggest a regional control on $\delta^{18}\text{O}$. We also cannot rule out minor contributions from the recharge frequency effect or in-karst disequilibrium fractionation. The high correlation between local and regional rainfall suggests that regardless of the exact mechanism, CC14-6 $\delta^{18}\text{O}$ is likely to be a good proxy for rainfall in the Murray-Darling Basin, at least under modern boundary conditions. It should therefore be possible to make inferences about past regional rainfall using stalagmites at this site.

Discussion

We test the hypothesis of local/regional rainfall control on speleothem $\delta^{18}\text{O}$, and the validity of the age model, by comparing the CC14-6 $\delta^{18}\text{O}$ record with rainfall records from the historical era. The nearest weather station at Burrinjuck Dam (BOM ID: 073007) is 10 km north-northwest of Careys Cave and has been operational since 1908. Prior to 1908 we use data from Fairlight Station (BOM ID: 070032), 29 km southeast of Careys Cave, operational since 1884. The rainfall reconstruction of Timbal and Fawcett (2013) comprises 11 SEA weather stations (not including Burrinjuck Dam or Fairlight Station) back to 1865.

The sampling resolution of CC14-6 is approximately annual. However, there were no visible annual laminations under visible or ultraviolet light that would allow an annually resolved record. Due to age model uncertainty and the risk of aliasing, direct comparisons with regional precipitation records at an annual level are not possible. Instead, we use 5-year running means instead to evaluate the recording fidelity of multi-year and decadal scale precipitation variability.

Figure 8 highlights the excellent relationship at the decadal to subdecadal scale between low $\delta^{18}\text{O}$ and wet periods, and high $\delta^{18}\text{O}$ and dry periods. A near perfect 1:1 relationship can be obtained by wiggle matching of just 3–5 years of the current age model, well within the approximately ± 20 age uncertainty. However, age model uncertainty also allows for alternative explanations within 2σ uncertainty envelopes, including a lagged response, out-of-phase relationship, antiphase relationship, and a one wet/dry cycle adjacent in-phase relationship. The shallow nature of the cave, and the fast response of formations becoming wet within a day or two after rainfall makes a lagged response unlikely. The excellent agreement between $\delta^{18}\text{O}$ and Mg/Ca mechanistically rules out out-of-phase and antiphase relationships between $\delta^{18}\text{O}$ and rainfall.

The mean distance between the median age model and the 2.5 and 97.5 percentiles is 18 years. A shift in the age model to a parallel age model one cycle different requires a shift of approximately 21 years (the periodicity in the Timbal and Fawcett rainfall reconstruction). Such a shift is therefore theoretically possible, but statistically unlikely according to the CC14-6 age model. However, a shift by one cycle can be achieved by altering the assumptions made in the construction of the age model. For example, if the stalagmite is assumed to be growing at the time of collection (2014) then the topmost $\delta^{18}\text{O}$ trough at 1.7–2.1 mm could represent wet conditions during the back to back La Niña events of 2010–11 and 2011–12, rather than the wet conditions around 1983–1984 indicated by the current median age model. Therefore, while we have confidence that the stalagmite $\delta^{18}\text{O}$ and Mg/Ca records are proxies for local and/or regional rainfall, recording decadal to sub-decadal scale wet and dry periods, 1:1 assignment of wet and dry decades remains a working hypothesis. Hereafter, we assume the median age model is correct but note a shift of wet and dry cycles by one period is possible.

Comparison with instrumental era rainfall

Assuming a median age model, good agreement can be found between high stalagmite $\delta^{18}\text{O}$ and dry periods around 1880, 1885–1900, 1915–1920, 1965–1970, and 1980–1985. Wet periods between 1865–1970, 1887, 1907–1911, 1945–1965 and 1970–1975 and 1985–1990 match well with low $\delta^{18}\text{O}$.

Discrepancies do exist between the CC14-6 $\delta^{18}\text{O}$ record and local and regional rainfall. The 1970–1975 $\delta^{18}\text{O}$ minima is relatively small compared to the 1950s and 1980 minima. This could represent a longer-term multi-decadal variability in $\delta^{18}\text{O}$, possibly related to source moisture effects or a low frequency local cumulative water balance (i.e. soil moisture) effect. Longer, more continuous records are required to infer any multi-decadal variability or periodicity with any certainty. Another area of disagreement is in the early 1940s where low stalagmite $\delta^{18}\text{O}$ is inconsistent with the 1937–1945 drought. If we assume that the stalagmite grew at a near-constant rate throughout deposition, rather than faster than usual between 20 and ~17 mm, then the base of the top section $\delta^{18}\text{O}$ record would be around 1950 rather than 1939 and the $\delta^{18}\text{O}$ record would no longer be in disagreement.

Which of the three major historical droughts are visible in the stalagmite? The Federation Drought (1895–1902) shows the clearest expression in the CC14-6 $\delta^{18}\text{O}$ record as a dry period. High $\delta^{18}\text{O}$ at 34.9 mm and 30.5 mm are both within the age model uncertainty. The World War II Drought (1937–1945) is either recorded as a wet period, or if linear growth throughout the top section of the stalagmite is assumed, is not recorded in the stable isotope record due to non-horizontal growth in the stalagmite following a change in drip location. Whether the Millennium Drought (1997–2010) is recorded is dependent on the assumptions made in the age model. The median age model suggests the drought was the cause of cessation of growth in CC14-6. However, if the stalagmite is assumed to be growing at the time of deposition then the positive $\delta^{18}\text{O}$ excursion between 8.3 and 5.1 mm is potentially the Millennium Drought.

Seasonality

Comparison of the CC14-6 $\delta^{18}\text{O}$ record with seasonally resolved precipitation records allows us to make initial hypotheses on seasonal biases in CC14-6 (Figure 8). The $\delta^{18}\text{O}$ time series was interpolated to 1-year resolution (180 to 113 data points) and correlated to the seasonal reconstructions of Timbal and Fawcett (2013). In the bottom section of the stalagmite significant (p -value >0.05) correlations occur between the annual $\delta^{18}\text{O}$ time series and rainfall during the SON and DJF seasons, summed rainfall during the JJASON, SONDJF and DJFMAM 6-month seasons, summed rainfall during all four 9-month seasons, and Annual rainfall. The lowest r -value (−0.59) and lowest p -value (>0.0001) are for SONDJF. This result

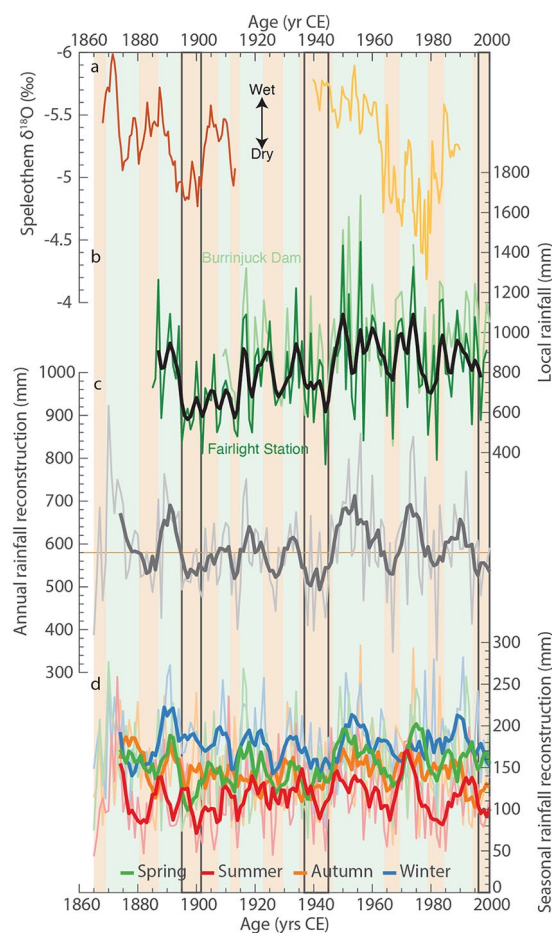


Figure 8. Comparison of the CC14-6 record with the historical record and regional reconstructions. (a) CC14-6 $\delta^{18}\text{O}$ record, top section in yellow, bottom section in red. (b) Local rainfall from Burrinjuck Dam (light green) and Fairlight Station (dark green with black 5-year running mean) weather stations. (c) Annual (gray) and 5-year running mean (gray) rainfall reconstruction of (Timbal and Fawcett, 2013) based on 11 long-term weather stations across south east Australia. (d) Seasonal breakdown of the (Timbal and Fawcett, 2013) rainfall reconstruction at annual (light colors, thinner lines) and 5-year running mean (darker colors, thicker lines) resolution. (Spring, SON, green; Summer, DJF, red; Autumn, MAM, orange; Winter, JJA, blue). Green and brown bars indicate periods where the 5 year running mean regional rainfall reconstruction was above/below 580 mm/yr. Black open boxes highlight the three major historical droughts in Australia: the Federation Drought (1895–1902), the World War II Drought (1937–1945) and the Big Dry or Millennium Drought (1997–2010).

suggests that CC14-6 could well be recording year-round rainfall, but with a potential bias toward spring and summer seasons. The top section of the stalagmite does not significantly correlate with any of the Timbal and Fawcett seasonal reconstructions, potentially due to age model errors at the base of the section described above or a smaller than expected negative excursion during the early 1970s.

A bias away from autumn and winter is somewhat unexpected given that evaporation exceeds precipitation in the summer months, and more rainfall falls in the winter. One possible explanation for this bias is increased growth rate during the warmer summer months. Alternatively, it might be related to how individual rainfall events contribute to karst recharge. A more detailed monitoring program is required to test these hypotheses.

Conclusion

High correlation between CC14-6 $\delta^{18}\text{O}$ and Mg/Ca records suggests that speleothems from Careys Cave, New South Wales act as an archive of local rainfall amount. Further, good correlations

between local and regional rainfall (CRU data), and previous studies on regional precipitation (Callow et al., 2014), suggests that speleothems from Careys Cave may also act as an archive of regional rainfall amount. The precise mechanism controlling speleothem $\delta^{18}\text{O}$ cannot be elucidated here, but is potentially a combination of different isotopic effects, including cumulative rainout along moisture trajectories, local rainfall amount, in-karst evaporation and in-karst non-equilibrium effects. All of these processes should result in higher $\delta^{18}\text{O}$ during drier conditions and lower $\delta^{18}\text{O}$ during wetter conditions. Additional cave-monitoring studies of drip-site hydrochemistry and local precipitation will enable further investigation into the controlling mechanisms of speleothem $\delta^{18}\text{O}$ recorded in the stalagmites at this site.

Speleothems from Careys Cave have demonstrated potential to record the timing, duration and intensity of past droughts in the Murray-Darling Basin beyond the limits of the historical record. Poor age control caused by low uranium concentration, normal for the region, was overcome by using a multi-proxy approach, incorporating radiocarbon modeling to constrain 20th century growth. The enhanced chronology shows a close correspondence between dry and wet decades in southeast Australian rainfall over much of the last 150 years. While 1:1 identification of individual wet and dry decades is not certain, it is likely that speleothem $\delta^{18}\text{O}$ from CC14-6 does record regional droughts, most likely the Federation Drought (1895–1902).

In the future, a combination of a thorough cave monitoring program and the extension of the speleothem record back through time will enable more reliable estimates of drought frequency in the region, and how it might have changed under a changing climate. This will allow investigation into potential common drivers of Murray-Darling Basin droughts, determine the climate sensitivity of rainfall in the basin, and ultimately inform local farmers and other policy makers, enabling them to increase resilience to potential future droughts.

Acknowledgements

We'd like to thank Geoff Kell and the Wee Jasper Reserves Trust for access to and sampling from Careys Cave, Laure Gauthiez-Putallaz and Paul Walczak for help with fieldwork, and an anonymous reviewer of an earlier version of this manuscript for their helpful comments.

Data availability

Data are available from the NOAA Paleoclimatology Database: <https://www.ncdc.noaa.gov/paleo/study/31794>, have been submitted to the SISAL database and are available from the author on request.

Funding

The author(s) disclosed receipt of the following financial support for the research, authorship, and/or publication of this article: We are grateful for financial support for this project from Steve Eggins, the Oceans and Atmospheres Cluster and Mike Gagan, all at the Research School of Earth Sciences, The Australian National University. MW was funded by an Australian Research Council Super Science Fellowship.

ORCID iD

Nick Scroxtan  <https://orcid.org/0000-0003-2315-9199>

References

- Akers PD, Brook GA, Railsback LB et al. (2019) Integrating U-Th, ^{14}C , and ^{210}Pb methods to produce a chronologically reliable isotope record for the Belize River Valley Maya from a low-uranium stalagmite. *The Holocene* 29(7): 1234–1248.
- Bureau of Meteorology (2016) *Climate Statistics for Australian Locations*. Melbourne, VIC: Bureau of Meteorology. Available at: <http://www.bom.gov.au/climate/data/index.shtml> (accessed 14 October 2016).
- Cai W, Purich A, Cowan T et al. (2014) Did climate change-induced rainfall trends contribute to the Australian Millennium Drought. *Journal of Climate* 27: 3145–3168.
- Cai Y (2005) Effect of dead carbon on the ^{14}C dating of the speleothem. *Chinese Science Bulletin* 50: 817–821.
- Callow N, McGowan H, Warren L et al. (2014) Drivers of precipitation stable oxygen isotope variability in an alpine setting, Snowy Mountains, Australia. *Journal of Geophysical Research: Atmospheres*, 119: 3016–3031.
- Cheng H, Edwards RL, Shen CC et al. (2013) Improvements in ^{230}Th dating, ^{230}Th and ^{234}U half-life values, and U–Th isotopic measurements by multi-collector inductively coupled plasma mass spectrometry. *Earth and Planetary Science Letters*, 371–372: 82–91.
- Chubb TH, Siems ST and Manton MJ (2011) On the decline of wintertime precipitation in the Snowy Mountains of Southeastern Australia. *Journal of Hydrometeorology* 12: 1483–1497.
- Coleborn K, Rau GC, Cuthbert MO et al. (2016) Solar-forced diurnal regulation of cave drip rates via phreatophyte evapotranspiration. *Hydrology and Earth System Sciences* 20: 4439–4455.
- Cuthbert MO, Baker A, Jex CN et al. (2014b) Drip water isotopes in semi-arid karst: Implications for speleothem paleoclimatology. *Earth and Planetary Science Letters* 395: 194–204.
- Cuthbert MO, Rau GC, Andersen MS et al. (2014a) Evaporative cooling of speleothem drip water. *Scientific Reports* 4: 5162.
- Dansgaard W (1964) Stable isotopes in precipitation. *Tellus* 16: 436–468.
- de Villiers S, Greaves M and Elderfield H (2002) An intensity ratio calibration method for the accurate determination of Mg/Ca and Sr/Ca of marine carbonates by ICP-AES. *Geochemistry, Geophysics, Geosystems* 3: 2001GC000169.
- Dixon BC, Tyler JJ, Lorrey AM et al. (2017) Low-resolution Australasian palaeoclimate records of the last 2000 years. *Climate of the Past* 13: 1403–1433.
- Fairchild IJ and Treble PC (2009) Trace elements in speleothems as recorders of environmental change. *Quaternary Science Reviews* 28: 449–468.
- Fairchild IJ, Borsato A, Tooth AF et al. (2000) Controls on trace element (Sr–Mg) compositions of carbonate cave waters: Implications for speleothem climatic records. *Chemical Geology* 166: 255–269.
- Fallon SJ, Fifield LK and Chappell JM (2010) The next chapter in radiocarbon dating at the Australian National University: Status report on the single stage AMS. *Nuclear Instruments and Methods in Physics Research Section B: Beam Interactions with Materials and Atoms* 268: 898–901.
- Genty D and Massault M (1997) Bomb ^{14}C recorded in laminated speleothems: Calculation of dead carbon proportion. *Radiocarbon* 39: 33–48.
- Geoscience Australia (2003) GEODATA TOPO 2.5M, Geoscience Australia, Canberra. Available at: <http://pid.geoscience.gov.au/dataset/ga/60804> (accessed 24 October 2020).
- Goede A, McDermott F and Hawkesworth C (1996) Evidence of younger dryas and neoglaciation cooling in a late quaternary palaeotemperature record from a speleothem in eastern Victoria, Australia. *Journal of Quaternary Science* 11: 1–7.
- Gouramanis C, De Deckker P, Switzer AD et al. (2013) Cross-continent comparison of high-resolution Holocene climate records from southern Australia—Deciphering the impacts of far-field teleconnections. *Earth-Science Reviews* 121: 55–72.

- Harris I, Jones PD, Osborn TJ et al. (2014) Updated high-resolution grids of monthly climatic observations – the CRU TS3.10 dataset. *International Journal of Climatology* 34: 623–642.
- Hellstrom J (2003) Rapid and accurate U/Th dating using parallel ion-counting multi-collector ICP-MS. *Journal of Analytical Atomic Spectrometry* 18: 1346–1351.
- Hogg AG, Hua Q, Blackwell PG et al. (2013) SHCal13 southern hemisphere calibration, 0–50,000 years cal BP. *Radiocarbon* 55: 1889–1903.
- Hua Q, Barbetti M and Rakowski AZ (2013) Atmospheric radiocarbon for the period 1950–2010. *Radiocarbon* 55: 2059–2072.
- Hutchinson MF, Stein JL, Stein JA et al. (2008) GEODATA 9 second DEM and D8: digital elevation model version 3 and flow direction grid 2008. *Record DEM-9S.v3*. Canberra: Geoscience Australia. Available at: <http://pid.geoscience.gov.au/dataset/ga/66006> (accessed 24 October 2020).
- Jaffey AH, Flynn KF, Glendenin LE et al. (1971) Precision measurement of half-lives and specific activities of ^{235}U and ^{238}U . *Physical Review C* 4: 1889–1906.
- Jex C, Acworth I, Azcurra C et al. (2012) Spatially dense drip hydrological monitoring and infiltration behaviour at the Wellington Caves, South East Australia. *International Journal of Speleology* 41: 285–298.
- Johnson KR, Hu C, Belshaw N et al. (2006) Seasonal trace-element and stable-isotope variations in a Chinese speleothem: The potential for high-resolution paleomonsoon reconstruction. *Earth and Planetary Science Letters* 244: 394–407.
- Lachniet MS (2009) Climatic and environmental controls on speleothem oxygen-isotope values. *Quaternary Science Reviews* 28: 412–432.
- Lougheed BC, Metcalfe B, Ninnemann US et al. (2018) Moving beyond the age–depth model paradigm in deep-sea palaeoclimate archives: Dual radiocarbon and stable isotope analysis on single foraminifera. *Climate of the Past* 14: 515–526.
- Ludwig KR (2012) *Isoplot 3.75: A Geochronological Toolkit for Microsoft Excel*. Berkeley Geochronology Center, Special Publication, p.5.
- Markowska M, Baker A, Andersen MS et al. (2016) Semi-arid zone caves: Evaporation and hydrological controls on $\delta^{18}\text{O}$ drip water composition and implications for speleothem paleoclimate reconstructions. *Quaternary Science Reviews* 131: 285–301.
- Markowska M, Baker A, Treble PC et al. (2015) Unsaturated zone hydrology and cave drip discharge water response: Implications for speleothem paleoclimate record variability. *Journal of Hydrology* 529: 662–675.
- Markowska M, Cuthbert MO, Baker A et al. (2020) Modern speleothem oxygen isotope hydroclimate records in water-limited SE Australia. *Geochimica et Cosmochimica Acta* 270: 431–448.
- Markowska M, Fohlmeister J, Treble PC et al. (2019) Modelling the ^{14}C bomb-pulse in young speleothems using a soil carbon continuum model. *Geochimica et Cosmochimica Acta* 261: 342–367.
- Matsuura K, Willmott C and Legates D (2009) WebWIMP, The Web-based, Water-Budget, Interactive, Modeling Program. Available at: <http://climate.geog.udel.edu/~wimp/> (accessed 14 October 2016).
- McBride JL and Nicholls N (1983) Seasonal relationships between Australian rainfall and the southern oscillation. *Monthly Weather Review* 111: 1998–2004.
- McDonald J and Drysdale RN (2007) Hydrology of cave drip waters at varying bedrock depths from a karst system in southeastern Australia. *Hydrological Processes* 21: 1737–1748.
- McDonald J, Drysdale R, Hill D et al. (2007) The hydrochemical response of cave drip waters to sub-annual and inter-annual climate variability, Wombeyan Caves, SE Australia. *Chemical Geology* 244: 605–623.
- McDonald J, Drysdale R, Hua Q et al. (2013) A 1,500 year south Australian rainfall record based on speleothem hydrological proxies. In: *The 19th national conference of the Australian meteorological and oceanographic society (AMOS)*, Melbourne Convention and Exhibition Centre, Melbourne, Australia, 11–13 February 2013.
- McDonald J, Drysdale RN and Hill D (2004) The 2002–2003 El Niño recorded in Australian cave drip waters: Implications for reconstructing rainfall histories using stalagmites. *Geophysical Research Letters* 31: 1–4.
- McGowan H, Callow JK, Soderholm J et al. (2018) Global warming in the context of 2000 years of Australian alpine temperature and snow cover. *Scientific Reports* 8: 4394.
- McGowan HA, Marx SK, Denholm J et al. (2009) Reconstructing annual inflows to the headwater catchments of the Murray River, Australia, using the Pacific Decadal Oscillation. *Geophysical Research Letters* 36: L06707.
- Murphy BF and Timbal B (2008) A review of recent climate variability and climate change in southeastern Australia. *International Journal of Climatology* 28: 859–879.
- Neukom R and Gergis J (2012) Southern hemisphere high-resolution palaeoclimate records of the last 2000 years. *The Holocene* 22: 501–524.
- Pook MJ, McIntosh PC and Meyers GA (2006) The synoptic decomposition of cool-season rainfall in the Southeastern Australian cropping region. *Journal of Applied Meteorology and Climatology* 45: 1156–1170.
- Rutledge H, Baker A, Marjo CE et al. (2014) Dripwater organic matter and trace element geochemistry in a semi-arid karst environment: Implications for speleothem paleoclimatology. *Geochimica et Cosmochimica Acta* 135: 217–230.
- Santrock J, Studley SA and Hayes JM (1985) Isotopic analyses based on the mass spectrum of carbon dioxide. *Analytical Chemistry* 57: 1444–1448.
- Schrag DP (1999) Rapid analysis of high-precision Sr/Ca ratios in corals and other marine carbonates. *Paleoceanography* 14: 97–102.
- Sinclair DJ (2011) Two mathematical models of Mg and Sr partitioning into solution during incongruent calcite dissolution. *Chemical Geology* 283: 119–133.
- Suess HE (1955) Radiocarbon concentration in modern wood. *Science* 122: 415–417.
- Tadros CV, Treble PC, Baker A et al. (2016) ENSO-cave drip water hydrochemical relationship: A 7-year dataset from South-Eastern Australia. *Hydrology and Earth System Sciences* 20: 4625–4640.
- Timbal B and Fawcett R (2013) A historical perspective on South-eastern Australian rainfall since 1865 using the instrumental record. *Journal of Climate* 26: 1112–1129.
- Trouet V and Van Oldenborgh GJ (2013) KNMI climate explorer: A web-based research tool for high-resolution paleoclimatology. *Tree-Ring Research* 69: 3–13.
- Tyler JJ, Mills K, Barr C et al. (2015) Identifying coherent patterns of environmental change between multiple, multivariate records: An application to four 1000-year diatom records from Victoria, Australia. *Quaternary Science Reviews* 119: 94–105.
- Ummenhofer CC, England MH, McIntosh PC et al. (2009) What causes southeast Australia's worst droughts? *Geophysical Research Letters* 36: L04706.
- Vance TR, Roberts JL, Plummer CT et al. (2015) Interdecadal Pacific variability and eastern Australian megadroughts over the last millennium. *Geophysical Research Letters* 42: 129–137.
- Vance TR, van Ommen TD, Curran MAJ et al. (2013) A millennial proxy record of ENSO and eastern Australian rainfall

- from the Law Dome ice core, East Antarctica. *Journal of Climate* 26: 710–725.
- Verdon-Kidd DC and Kiem AS (2009) Nature and causes of protracted droughts in southeast Australia: Comparison between the Federation, WWII, and Big Dry droughts. *Geophysical Research Letters* 36: L27707.
- Wassenburg JA, Riechelmann S, Schröder-Ritzrau A et al. (2020) Calcite Mg and Sr partition coefficients in cave environments: Implications for interpreting prior calcite precipitation in speleothems. *Geochimica et Cosmochimica Acta* 269: 581–596.
- Webb M, Dredge J, Barker PA et al. (2014) Quaternary climatic instability in south-east Australia from a multi-proxy speleothem record. *Journal of Quaternary Science* 29: 589–596.
- Zhou H, Zhao X, Qing W et al. (2011) Speleothem-derived Asian summer monsoon variations in Central China, 54–46 ka. *Journal of Quaternary Science* 26: 781–790.